2024 17th United Conference on Millemetre Waves and Terahertz Technologies (UCMMT) | 979-8-3315-3022-8/24/$31.00 ©2024 IEEE | DOI: 10.1109/UCMMT62975.2024.10737832

Multi-Dimensional Multi-Polarization Millimeter-Wave Antenna Array for Vehicle Communication

Zhonghe Zhang[1], Jing-Yu Lin[2], Sai-Wai Wong[1]*, Youquan Wen[1], Chaoyun Song[1], Yejun He[1]
1. College of Electronics and Information Engineering, Shenzhen University, Shenzhen, China
2. Institute of Electromagnetics and Acoustics, Xiamen University, Xiamen, China.
2150432016@email.szu.edu.cn, linjingyu@xmu.edu.cn, wongsaiwai@ieee.org,
wenyouquan2022@email.szu.edu.cn, chaoyun.song@kcl.ac.uk, heyejun@126.com

***Abstract*- This paper proposes a millimeter-wave antenna array tailored for vehicular communication, capable of supporting multi-dimensional and multi-polarization communication requirements. The antenna consists of a fully metallic cavity structure and PCB feeding structure, supporting dual band operation. At 27.24 GHz, the antenna achieves circular polarization in the top direction for V2I communication. At 28.1 GHz, the antenna achieves vertical polarization in the forward direction for V2V communication. A 1×4 antenna array is fabricated to achieve high-gain beam coverage in different directions. Suitable for 5G-based vehicular IoT applications.**

I. INTRODUCTION

The fifth generation (5G) vehicular networking offers significant advantages. Its high-speed transmission, low latency, and high reliability greatly enhance the efficiency and safety of vehicle communication [1]-[3]. This advanced technology enables vehicles to process real-time data swiftly, driving advancements in intelligent transportation and autonomous driving. Additionally, 5G networks' ability for multiple connections and efficient interconnectivity provides a solid foundation for a wide range of applications in vehicular IoT [4]. To enhance communication quality, dual band antennas with small frequency ratio have been proposed. In [5], orthogonal linear polarization in two frequency bands was achieved on the patch through analysis of characteristic modes. In [6], a vehicular antenna system was developed that uses two adjacent frequency bands to create cross-shaped beam patterns, enabling both V2V2 and V2I communications. Dual circular polarization within two frequency bands was implemented on the patch antenna [7]. Building upon this foundation, a new method achieving dual-band dual-sense circular polarization within two frequency bands has been proposed [8]. For multi-port antennas, achieving isolation between ports is an effective way to enhance communication quality. Using metasurface structures [9]-[16] to isolate different antenna elements or arrays is a proven method. Many researchers have explored this, including studies on metasurface bandgap structures and metasurface unit cells, particularly in the millimeter wave and terahertz frequency bands, where metasurfaces have shown significant

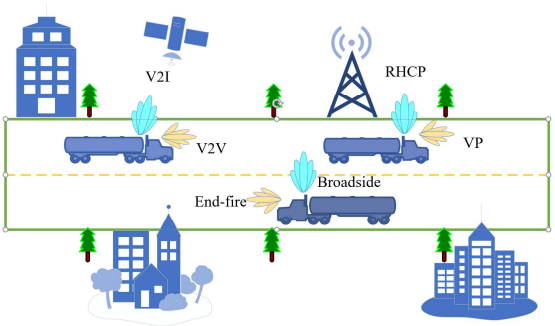

Fig. 1. Diagram of multi-beam multi-polarization vehicle communication.

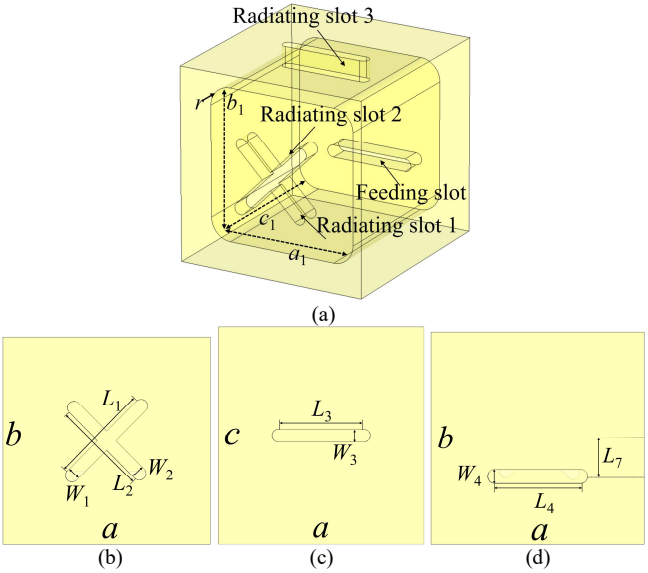

Fig. 2. Antenna structure. (a) 3-D view.(b) Front view. (c) Top view. (d) Rear view. Physical dimensions (units: mm): L_1 = 4.4, L_2 = 4.2, L_3 = 3.9, L_4 = 3.7, a= 9.4, a_1= 7.4, b= 9.4, b_1= 7.4, c= 9.9, c_1= 7.9,W_1 = 0.6, W_2 = 0.6, W_3 = 0.6, W_4 = 0.6.

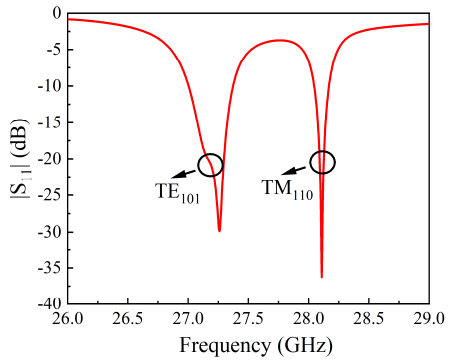

Fig. 3. Simulated parameters of $|S_{11}|$.

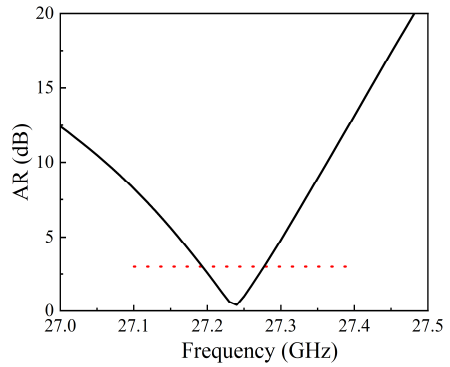

Fig. 4. Simulated parameters of AR.

effectiveness. It is noteworthy that most multi-frequency antennas only achieve beam coverage in a single direction. For instance, V2I communication often takes place at the top of vehicles, whereas V2V communication typically occurs at the front, a capability seldom realized by relevant antennas.

II. Design of Antenna

Fig. 1 depicts a diagram of multi-beam multi-polarization vehicle communication: the antenna radiates right-hand circular polarization in the broadside direction and linear polarization in the end-fire direction. This allows the vehicle to maintain communication not only with the vehicle in front while driving but also with satellites positioned above.

Antenna structure as shown in Fig. 2: The antenna consists of an empty metallic cavity with slots on different surfaces. Fig. 2(a) provides a 3-D view, Fig. 2(b) shows the front view where intersecting radiation slots achieve circular polarization beams. Fig. 2(c) displays the top view where linear polarization beams are achieved, and Fig. 2(d) presents the rear view showcasing feeding slots.

The antenna's different frequencies are achieved by simultaneously exciting different modes of the cavity. Fig. 3 displays the $|S_{11}|$ parameter of the antenna. At 27.24 GHz,

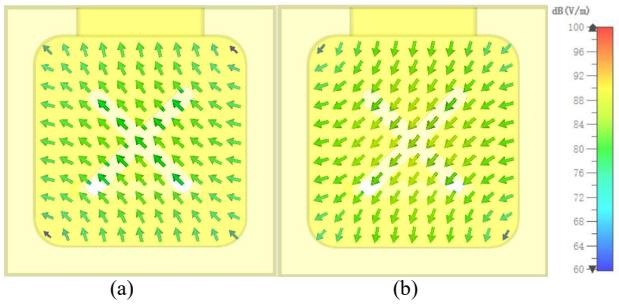

Fig. 5. Cavity internal electric field at 27.24 GHz. (a) t=0. (b) t=T/4.

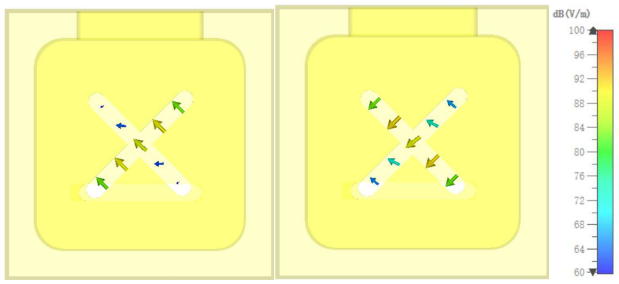

Fig. 6. Cavity slot electric field at 27.24 GHz. (a) t=0. (b) t=T/4.

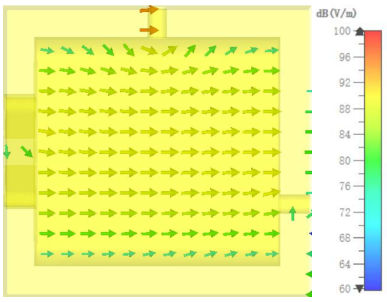

Fig. 7. Cavity internal electric field at 28.1 GHz.

circular polarization is generated by the antenna's degenerate mode TE_{101}; at 28.1 GHz, linear polarization is generated by the antenna's TM_{110} mode. The antenna axial ratio as shown in Fig. 4, is below 3dB at 27.24 GHz, indicating effective circular polarization performance.

The circular polarization of the antenna is generated by the degenerate modes of the antenna. Inside the metal cavity, the electric field directions of the two modes are orthogonal. Fig. 5(a) shows the electric field direction of the antenna at time t = 0. After a 90° phase shift, as shown in Fig. 5(b), the electric field direction inside the cavity has rotated by 90°, which meets the conditions for circularly polarized beam generation. Fig. 6 shows the electric field across the long edge direction of the cavity slot at 27.24 GHz, which excites the antenna's radiation performance. We can observe that this is consistent with the electric field direction inside the cavity depicted in

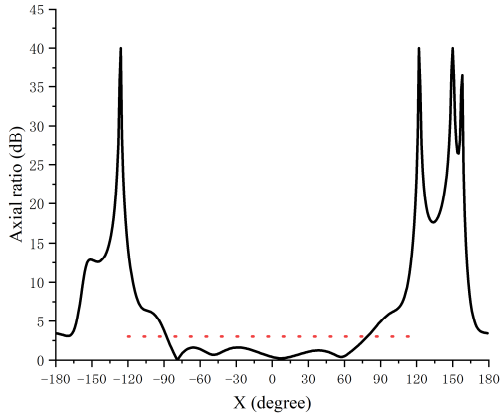

(a)

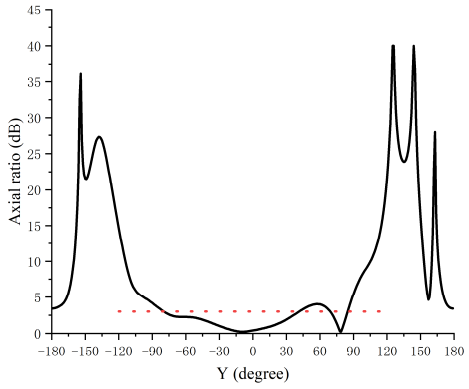

(b)

Fig. 8. Simulated AR beamwidth of the proposed antenna. (a)xoz plane. (b) yoz plane.

Fig. 5. The overlapping of mutually perpendicular electric field directions, with a 90° phase difference, results in the generation of a right-hand circularly polarized beam.

As depicted in Fig. 7, at 28.1 GHz, the electric field inside the cavity aligns with the radiation direction of the field produced by the slot, resulting in the excitation of a vertically polarized beam in the end-fire direction of the antenna.

As shown in Fig. 8, the antenna maintains a relatively wide axial ratio performance in the radiation direction, achieving good beam coverage in the end-fire direction. It provides over 150° of circularly polarized beam coverage in the xoz plane and over 100° in the yoz plane. The axial ratio in the yoz plane is slightly lower due to the feed structure being in the same plane, leading to a decrease in circular polarization performance in the yoz plane due to irregular feed structure and misaligned ground plane. However, this can be avoided in practical antenna applications.

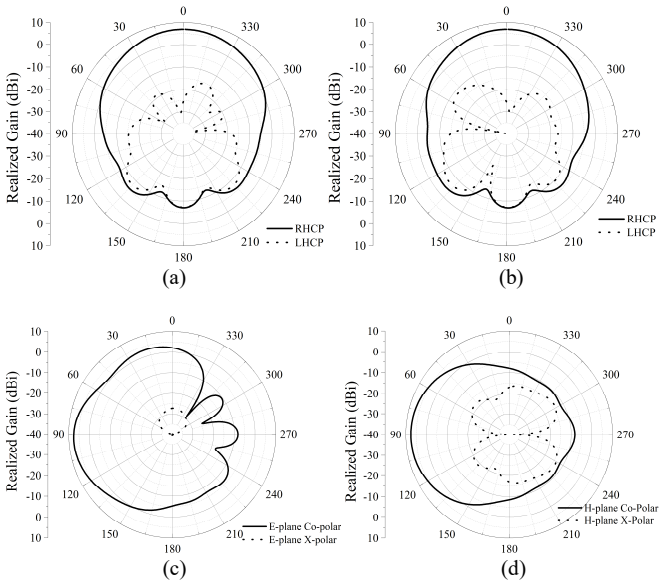

Fig. 9. Simulated antenna radiation patterns. (a) xoz plane 27.24 GHz. (b) yoz plane 27.24 GHz. (c) yoz plane 28.1 GHz. (d) xoy plane 28.1 GHz.

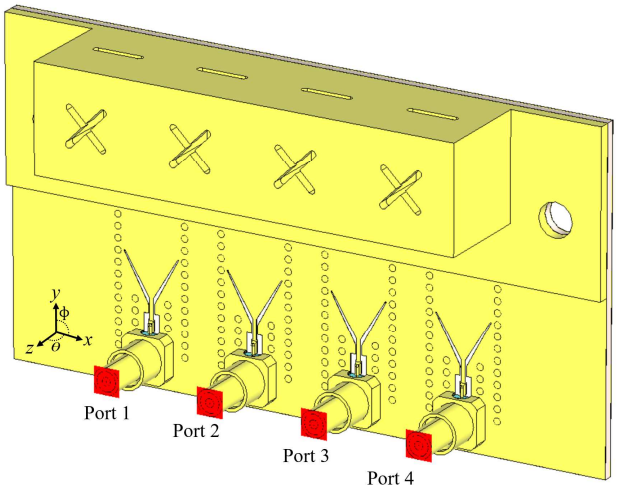

Fig. 10. Simulated antenna array structure.

The radiation patterns of the antenna unit are shown in Fig. 9. Fig. 9(a) and Fig. 9(b) depict the circularly polarized radiation patterns of the antenna at 27.24 GHz, with the beam directed towards the +z direction. The actual gain of the antenna in this direction is 6.61 dBi. Fig. 9(c) and Fig. 9(d) show the circularly polarized radiation patterns of the antenna at 27.24 GHz, with the beam directed towards the +x direction. The actual gain of the antenna in this direction is 7.71 dBi. Additionally, the antenna maintains cross-polarization performance below -20 dBi across different frequency bands. This indicates that the antenna achieves beam coverage in different directions and polarizations within the same aperture.

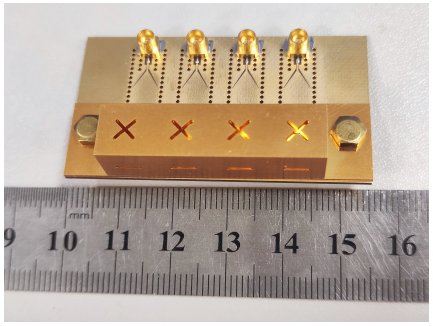

Fig. 11. Fabricated prototype.

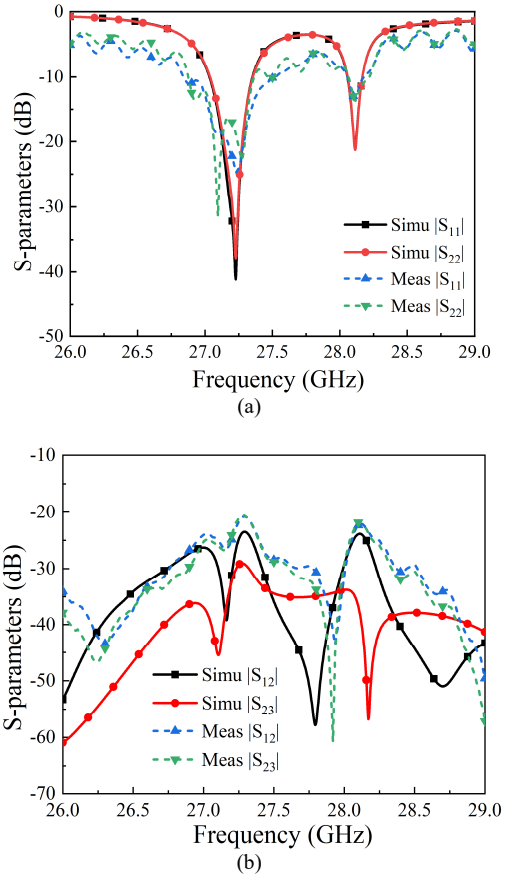

Fig. 12. Simulated and measured S-parameters of the antenna array.

III. Design of Antenna Array

Simulated antenna array structure is shown in Fig. 10. The antenna is entirely made of metal, but the traditional RF chip and signal processing modules are integrated into a PCB. To integrate with the conventional PCB system, a substrate-integrated waveguide is used to feed the metal cavity antenna.

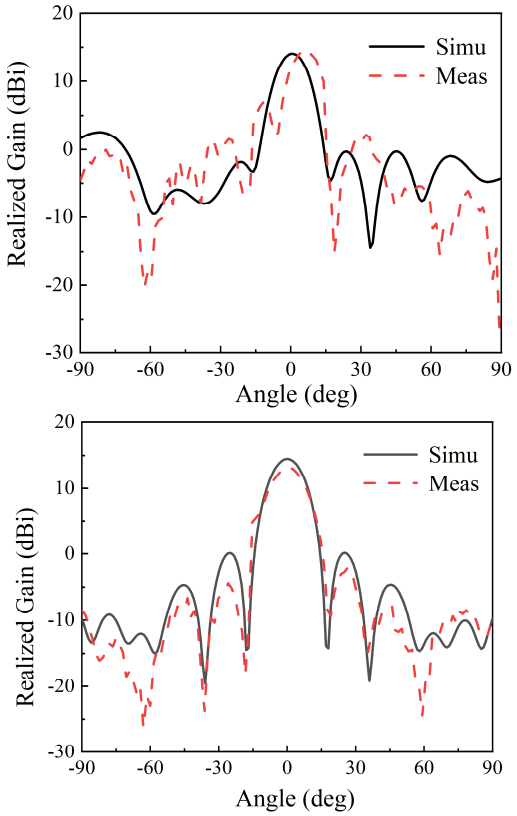

Fig. 13. Simulated and measured antenna array radiation patterns. (a) 27.24 GHz. (b) 28.1 GHz.

The fabricated prototype, as shown in Fig. 11, utilizes a PCB substrate for antenna feeding. Screws are added on both sides of the metallic cavity and between the substrate layers to reinforce the structure. The surface of the metallic cavity is gold-plated to prevent rusting. When simultaneously exciting four feed probes, the antenna achieves circular polarization beam coverage in the top direction and linear polarization beam coverage on the side. The four array units achieve high-gain coverage in two directions.

As shown in Fig. 12, the simulated and measured S-parameters of the antenna array indicate that each port is independent, and return loss parameters for each port were tested. The port structure is symmetrical, with both the measured and simulated return losses for ports 1 and 2 being below -10 dB, meeting the requirements at 27.24 GHz and 28.1 GHz. Minor discrepancies are attributed to inaccuracies in fabrication and testing soldering. The isolation between different ports also demonstrates this symmetry, with isolation between ports 1 and 2 below -20 dB, and similarly between ports 2 and 3. The measured and simulated results are in close agreement. Traditional phased array or MIMO antennas require port isolation of -15 dB or better. This design holds broad application value.

Simulated and measured antenna array radiation patterns as shown in Fig. 13. The radiation pattern achieving circular polarization at the top is shown in Fig. 13(a). The antenna resonates at 27.24 GHz, with a simulated peak gain of 14.4 dBi and a measured peak gain of 14.37 dBi. The main beam deviates approximately 5°, which is attributed to measurement environment errors. The radiation pattern achieving linear polarization on the side is shown in Fig. 13(b). The antenna resonates at 28.1 GHz, with a simulated peak gain of 14.48 dBi and a measured peak gain of 13.2 dBi. The frequency ratio of 1.03 between the two frequencies enabled a good beam separation within a small frequency ratio.

IV. Conclusion

This paper proposes a multi-beam, multi-polarization array antenna for millimeter-wave vehicular communication. The antenna features a fully metallic cavity structure, employing different cavity modes at two frequencies: the TE_{101} mode for circular polarization beam coverage at the top and the TM_{110} mode for vertical polarization beam coverage on the side. This allows the antenna to achieve high-gain beam coverage in multiple dimensions and polarizations using a single structure.

Acknowledgment

This work was supported in part by the National Key Research and Development Program of China under Grant 2023YFE0107900; in part by the National Natural Science Foundation of China under Grant 62071306

References

[1] J. Huang, C. -X. Wang, H. Chang, J. Sun and X. Gao, "Multi-Frequency Multi-Scenario Millimeter Wave MIMO Channel Measurements and Modeling for B5G Wireless Communication Systems," *IEEE J. Sel. Areas Commun.*, vol. 38, no. 9, pp. 2010-2025, Sept. 2020.

[2] J. Guo, Y. Hu and W. Hong, "A 45° Polarized Wideband and Wide-Coverage Patch Antenna Array for Millimeter-Wave Communication," *IEEE Trans. Antennas Propag.*, vol. 70, no. 3, pp. 1919-1930, Mar. 2022.

[3] B. B. Ai, A. F. Molisch, M. Rupp, Z. -D. Zhong, "5G key technologies for smart railways," *Proceedings IEEE*, vol. 108, no. 6, pp. 856-893, Jun. 2020.

[4] Y. Bi, Y. Li, H. Wong, B. Xiao, L. Ge and J. Wang, "A Millimeter-Wave Wideband Antenna Module With Switchable Fan-Beam Radiation for Wide Coverage of 5G IoT Applications," *IEEE Internet Things J.*, vol. 10, no. 23, pp. 20969-20983, 1 Dec. 2023.

[5] D. Fazal and Q. U. Khan, "Dual-Band Dual-Polarized Patch Antenna Using Characteristic Mode Analysis," *IEEE Trans. Antennas Propag.*, vol. 70, no. 3, pp. 2271-2276, Mar. 2022.

[6] Z. Zhang, S. -W. Wong, Y. Wen, S. -Q. Zhang, W. Li and Y. He, "A Full-Metal Dual-Band Millimeter-Wave Antenna Array With Concomitant Multifold Orthogonal Beamforming for V2V and V2I Communications," *IEEE Trans. Veh. Technol.*, vol. 73, no. 7, pp. 10381-10389, Jul. 2024.

[7] N. -W. Liu, L. Zhu, Z. -X. Liu, Z. -Y. Zhang and G. Fu, "Frequency-Ratio Reduction of a Low-Profile Dual-Band Dual-Circularly Polarized Patch Antenna Under Triple Resonance," *IEEE Antennas Wireless Propag. Lett.*, vol. 19, no. 10, pp. 1689-1693, Oct. 2020.

[8] W. -W. Chen, Q. -S. Wu and X. Zhang, "Quad-Mode Dual-Band Dual-Sense Circularly Polarized Microstrip Patch Antenna," *IEEE Antennas Wireless Propag. Lett.*, vol. 23, no. 5, pp. 1503-1507, May. 2024.

[9] M. Alibakhshikenari et al., "A Comprehensive Survey on "Various Decoupling Mechanisms With Focus on Metamaterial and Metasurface Principles Applicable to SAR and MIMO Antenna Systems"," *IEEE Access*, vol. 8, pp. 192965-193004, Nov. 2020.

[10] M. Alibakhshikenari, B. S. V. B, and E. L. A. "Study on isolation and radiation behaviours of a 34×34 array-antennas based on SIW and metasurface properties for applications in terahertz band over 125–300 GHz." *Optik, International Journal for Light and Electron Optics,* Vol. 206, no. 163222. Mar. 2020.

[11] M. Alibakhshikenari, et al. "Isolation Enhancement of Densely Packed Array Antennas with Periodic MTM-Photonic Bandgap for SAR and MIMO Systems." *IET Microwaves Antennas & Propagation* (2019). Vol. 14, no. 3, pp. 183 - 188, Feb. 2020.

[12] M. Alibakhshikenari, M. Khalily, B. S. Virdee, C. H. See, R. A. Abd-Alhameed and E. Limiti, "Mutual-Coupling Isolation Using Embedded Metamaterial EM Bandgap Decoupling Slab for Densely Packed Array Antennas," *IEEE Access*, vol. 7, pp. 51827-51840, 2019.

[13] M. Alibakhshikenari, M. Khalily, B. S. Virdee, C. H. See, R. A. Abd-Alhameed and E. Limiti, "Mutual Coupling Suppression Between Two Closely Placed Microstrip Patches Using EM-Bandgap Metamaterial Fractal Loading," IEEE Access, vol. 7, pp. 23606-23614. 2019.

[14] M. Alibakhshikenari, et al. "Antenna Mutual Coupling Suppression Over Wideband Using Embedded Periphery Slot for Antenna Arrays." *Electronics*. vol. no. 9, pp. 198. 2018.

[15] M. Alibakhshikenari, , et al. "Study on isolation improvement between closely-packed patch antenna arrays based on fractal metamaterial electromagnetic bandgap structures." *IET Microwaves Antennas & Propagation*. vol. 12, no. 14, pp. 2241–2247, Nov. 2018.

[16] M. Alibakhshikenari, et al. "Meta-Surface Wall Suppression of Mutual Coupling between Microstrip Patch Antenna Arrays for THz-Band Applications." *Progress in Electromagnetics Research Letters,* vol. 75, pp. 105-111,2018.